Title:

Curiosity at Gale crater, Mars: Characterization and analysis of the Rocknest sand shadow

Authors:

D. F. Blake[1]*, R. V. Morris[2], G. Kocurek[3], S. M. Morrison[4], R. T. Downs[4], D. Bish[5], D. W. Ming[2], K. S. Edgett[6], D. Rubin[7], W. Goetz[8], M. B. Madsen[9], R. Sullivan[10], R. Gellert[11], I. Campbell[11], A. H. Treiman[12], S.M. McLennan[13], A. S. Yen[14], J. Grotzinger[15], D. T. Vaniman[16], S. J. Chipera[17], C. N. Achilles[2], E. B. Rampe[2], D. Sumner[18], P-Y Meslin[19], S. Maurice[19], O. Forni[19], O. Gasnault[19], M. Fisk[20], M. Schmidt[21], P. Mahaffy[22], L. A. Leshin[23], D. Glavin[22], A. Steele[24], C. Freissinet[22], R. Navarro-González[25], R. A. Yingst[16], L. C. Kah[26], N. Bridges[27], K. W. Lewis[28],T. F. Bristow[1], J. D. Farmer[29], J. A. Crisp[14], E. M. Stolper[15], D. J. Des Marais[1], P. Sarrazin[30] and the MSL Science Team[31]

Affiliations:

[1]NASA Ames Research Center, Moffett Field, CA 94035 USA.

[2]NASA Johnson Space Center, Houston, TX USA.

[3]Department of Geological Sciences, University of Texas, Austin, TX USA.

[4]Department of Geology, University of Arizona, Tucson, AZ USA.

[5]Department of Geological Sciences, Indiana University, Bloomington, IN USA.

[6]Malin Space Science Systems, San Diego, CA USA.

[7]University of California, Santa Cruz, Santa Cruz, CA USA.

[8]Max-Planck-Institut für Sonnensystemforschung, 37191 Katlenburg-Lindau, Germany.

[9]Niels Bohr Institute, University of Copenhagen, 2100 Copenhagen, Denmark.

[10]Center for Radiophysics and Space Research, Cornell University, Ithaca, NY USA.

[11]University of Guelf, Guelph, Ontario, N1G2W1, Canada.

[12]Lunar and Planetary Institute, Houston, TX USA.

[13]SUNY Stony Brook, Stony Brook, NY USA.

[14]Jet Propulsion Laboratory/California Institute of Technology, Pasadena, CA USA.

[15]California Institute of Technology, Pasadena, CA USA.

[16]Planetary Science Institute, Tucson, AZ USA.

[17]Chesapeake Energy, Oklahoma City, OK USA.

[18]University of California, Davis, CA USA.

[19] Institut de Recherche en Astrophysique et Planétologie (IRAP), UPS-OMP-CNRS, Toulouse, France.

[20]Oregon State University, Corvallis, OR USA.

[21]Finnish Meteorological Institute, Helsinki, Finland.

[22]NASA Goddard Space Flight Center, Greenbelt, MD USA.

[23]Rensselaer Polytechnic Institute, Troy, NY USA.

[24]Geophysical Laboratory, Carnegie Institution of Washington, Washington, DC USA.

[25]University Nacional Autonóma de México, Ciudad Universitaria, 04510 México D.F. 04510 Mexico.

[26]Department of Earth and Planetary Sciences, University of Tennessee, Knoxville, TN USA.

[27]The Johns Hopkins University Applied Physics Laboratory, Laurel, MD USA.

[28]Princeton University, Princeton, NJ USA.

[29]Arizona State University, Phoenix, AZ USA.

[30]SETI Institute, Mountain View, CA USA.

[31]See Supplementary Materials for the full list of the MSL team.

*Correspondence to: david.blake@nasa.gov

Abstract:

The Rocknest aeolian deposit is similar to aeolian features analyzed by the Mars Exploration Rovers (MER) *Spirit* and *Opportunity*. The fraction of sand <150 μm in size contains ~55% crystalline material consistent with a basaltic heritage, and ~45% X-ray amorphous material. The amorphous component of Rocknest is Fe-rich and Si-poor, and is the host of the volatiles (H_2O, O_2, SO_2, CO_2, and Cl) detected by the Surface Analysis at Mars (SAM) instrument and of the fine-grained nanophase oxide (npOx) component first described from basaltic soils analyzed by MER. The similarity between soils and aeolian materials analyzed at Gusev crater, Meridiani Planum and Gale crater implies locally sourced, globally similar basaltic materials, or globally and regionally sourced basaltic components deposited locally at all three locations.

Introduction:

The Mars Science Laboratory rover *Curiosity* began exploring the surface of Mars on August 6, 2012, UTC; until September 13, 2012, it conducted an initial engineering checkout of its its mobility system, arm and science instruments. *Curiosity* spent Sols 57-

100 *(1)* at a location named "Rocknest," collecting and processing five scoops of loose, unconsolidated materials extracted from an aeolian sand shadow *(2)*.

Five scoops of material from the Rocknest sand shadow were individually collected and sieved (<150 μm) by the Sample Acquisition, Sample Processing and Handling – Collection and Handling for In situ Martian Rock Analysis (SA/SPaH-CHIMRA) instrument (*3*). Scoops 1 and 2 were processed by CHIMRA and discarded to reduce (by entrainment and dilution) any terrestrial organic contamination that may have remained after a thorough cleaning on Earth (*4*) and to coat and "passivate" the interior surfaces of the collection device with Mars dust. Portions (40-50 mg.) of scoops 3 and 4 were delivered to the Chemistry and Mineralogy (CheMin) instrument (*5*) and the "observation tray," a 7.5 cm diameter flat Ti-metal surface used for imaging and analyzing scooped and sieved material with *Curiosity's* arm and mast instruments. Portions of scoop 5 were delivered to both CheMin and the SAM quadrupole mass spectrometer/gas chromatograph/tunable laser spectrometer suite of instruments (*6*).

We describe the physical sedimentology of Rocknest and suggest possible sources for the material making up the sand shadow. We utilize Alpha-Particle X-ray Spectrometer (APXS) and CheMin data to determine the amounts and chemistry of the crystalline and amorphous components of the sand shadow, and compare these results to global soil measurements from the MER rovers and to basaltic martian meteorites analyzed on Earth.

Results

Description and interpretation of the Rocknest sand shadow

The Rocknest sand shadow (*7*) is an accumulation of wind-blown sediment deposited in the lower-velocity lee of an obstacle in the path of the wind. The orientation of the sand shadow indicates that the constructive winds were from the north. The surface is composed of dust-coated, predominantly rounded, very coarse (1-2 mm) sand grains (Fig. 1a). Trenches created during the scooping show that these larger grains form an armored surface ~2-3 mm in thickness (Fig. 1b). Beneath the armored surface, the bedform interior consists of finer-grained material whose size distribution extends through the resolution limit of Mars Hand Lens Imager (MAHLI) images (~30 μm/pixel under the conditions of the observation) (*8*). Because of CHIMRA's 150 μm sieve, the larger grains that armor the surface could not be analyzed by CheMin.

Coarse sand grains that fell from the crust into the scoop-troughs lost their dust coating and show diversity in color, luster, and shape. Among the grains are gray and red lithic fragments, clear/translucent crystal fragments, and spheroids with glassy luster (Fig. 1c). Some grains showed bright glints in the martian sunlight, suggesting specular reflections from mineral crystal faces or cleavage surfaces (similar features were observed by the Optical Microscope onboard the Mars Phoenix Lander (*9*)). MAHLI images of a sieved portion of material deposited on the observation tray (*3*) showed a variety of particle types from clear to colored to dark, angular to spherical, and dull to glassy-lustered, (Fig. 1d).

During the scooping process, fragments of the armored surface were cohesive to the extent that "rafts" of surface crust were laterally compressed and displaced forward, and fragments of the crust fell into the scoop hole as cohesive units (Fig. 1b). The surface crust was also fractured and broken into 'rafts' during scuffing by rover wheels (a process by which an excavation is made into the subsurface of unconsolidated regolith by rotating a single rover wheel). Material beneath the crust also had some cohesion, as shown by the over-steep walls of the scoop scars (much greater than the angle of repose and vertical in some cases).

The sand shadow has a discernable internal structure. On the headwall and flanks of each scoop trench, a lighter-tone layer is apparent ~1 cm beneath and parallel to the dune surface (Fig. 1b). The origin of the layering is not understood, and three hypotheses are viable. First, the layering may represent changes in bulk composition or grain size that occurred during deposition. Second, the layering may be the result of changes in oxidation state or other chemical properties that occurred after deposition, in which case the conformable nature of the banding and the surface of the sand shadow reflect depth-dependent post-depositional chemical processes. Finally, the layering may represent zones richer or poorer in light-toned dust, reflecting times of lesser or greater sand accumulation relative to the air-fall dust.

The aeolian bedform at Rocknest is quite similar to coarse-grained ripples encountered at Gusev by the MER rover *Spirit* (*10, 11*) and at Meridiani Planum by MER rover *Opportunity* (*12, 13*) in that a coarse-grained, indurated, dust-coated surface overlies an

interior of markedly finer sediment. Coarse-grained ripples on Earth typically consist of a surface veneer of coarse grains and a finer grained interior (*7, 14*), and the martian bedforms have been considered analogous features (*13, 15*). The spatial grain-size sorting within coarse-grained ripples is thought to arise because of the short grain excursion length of the coarse grains traveling in creep and the much longer excursion length of finer saltating grains (*16*). With ripple migration, coarse grains are recycled through the bedform and become concentrated on the ripple surface where impacts from saltating grains tend to buoy the grains upward.

Although the dynamics of sand shadows differ from those of coarse-grained ripples, and sand shadows on Earth do not characteristically show a coarse-grained surface, similar dynamics may arise owing to the mix-load transport of grains in creep and saltation. Alternate interpretations are also possible. First, the coarse-grained surface could represent a lag formed as winds deflated finer grains. However, the paucity of coarse grains within the interior indicates that an unreasonable amount of deflation would have had to occur to produce the veneer. Second, the coarse-grained veneer could represent the terminal growth phase of the bedform. Because the size of a sand shadow is fixed by the upwind obstacle size (*17*), once the terminal size is approached, the lower wind speeds that characterize the wake and allow for deposition of finer sediment are replaced by wind speeds that approach the unmodified (primary) winds. At this point there would be selective deposition of coarse grains traveling in creep while finer saltating grains would bypass the bedform. Third, the sand shadow could have formed largely by the more readily transported fine saltation load, but as the area became depleted in finer grains,

more of the residuum of coarser grains would be incorporated into transport, with the coarse-grained surface arising through subsequent deflation.

None of these interpretations explains the general absence of observed coarse grains in the interior; the contrast in grain size between the surface and the interior is more marked in the Rocknest sand shadow and in some of the coarse-grained ripples observed by MER than in many Earth examples. This may reflect the greater impact energy of saltating grains on Mars compared to Earth, and their ability to transport disproportionally larger grains in creep (*18*). Regarding the apparent absence of interior coarse grains, the small scooped areas may not be representative of the entire bedform and interior horizons of coarse grains could easily have been bypassed. In addition, as seen with coarse-grained ripples on Earth, the amount of coarse sediment occurring in the interior varies and decreases with the supply coarse grains.

Regardless of the origin of the coarse-grained surface, this armored surface would stabilize the bedform during all but the strongest wind events. In turn, the armored surface would allow time for surface induration to develop, further stabilizing the sand shadow. The similarity of the armoring and induration of the sand shadow at Rocknest to coarse-grained ripples encountered by Spirit and Opportunity suggests that the processes of grain transport and stabilization are similar across equatorial Mars, and that Mars' winds (in recent eras) rarely were strong enough to transport sand grains of 1-3 mm diameter. To move the grains at the current atmospheric pressure of 0.02 kg/m^3, the wind velocities would need to be ~36 m/s (80 mph) and ~ 52 m/s (116 mph) with and

without saltation, respectively. Under conditions of high obliquity, during which time the atmospheric pressure could increase to 0.04 kg/m^3, these values would decrease to 26 m/s (58 mph) and ~ 37 m/s (83 mph) respectively (see Materials and Methods). The potential antiquity of the Rocknest sand shadow is highlighted by comparing it with granule ripples on Meridiani Planum, where cratering post-dates a field of pristine granule ripples and the crater count suggests an age of 50-200 ka *(19)*.

Mineralogy of the Rocknest sand shadow

Analysis and interpretation of the mineralogy of the Rocknest sand shadow is given in a companion paper (*20*). Rocknest consists of both crystalline and X-ray amorphous components. The crystalline component is basaltic, comprised of plagioclase feldspar, forsteritic olivine, and the pyroxenes augite and pigeonite (*20*). All of the minor phases are consistent with a basaltic heritage with the exception of anhydrite and hematite. By constraining the compositions of the individual crystalline phases on the basis of their measured unit-cell parameters, the chemical compositions of the minerals of Rocknest were determined (*21, 22*).

The crystalline component of Rocknest is chemically and mineralogically similar to that inferred for martian basalts across the planet, and many of the basalts found in martian meteorites (Table 1) and, apart from somewhat lower Fe and K, broadly similar to estimates of the average Martian crust (*23*). These basalts all contain (or have chemical compositions consistent with) the minerals olivine, augite, pigeonite and plagioclase feldspar. The mineral proportions of the crystalline component of Rocknest are virtually

identical to those calculated for the unaltered Adirondack class basalts from Gusev Crater (CIPW normative mineralogy from their APXS analyses (Table 1) (*24, 25*). Chemically, the mafic minerals of the Rocknest sediment (olivine, augite, and pigeonite) are all consistent with high-temperature chemical equilibria among Ca, Fe, and Mg at 1050±75C (Fig. 2). This consistency with chemical equilibria suggests, but does not prove, that these minerals and the plagioclase feldspar all derived from a common basaltic source rock, which was broken down into individual grains or lithic fragments, and transported to Rocknest from regional source areas.

Bulk Chemistry of the Rocknest sand shadow

APXS provided an independent means of determining bulk chemistry of material in the Rocknest sand shadow. A measurement was made in a wheel scuff named Portage which was largely devoid of surface crust (Fig. 1a). The chemical composition (taking into account analytical uncertainty) is within 2σ of MER APXS analyses of basaltic soils (Table 2). The APXS chemistry of basaltic soils analyzed by the MER rovers at Gusev crater and Meridiani Planum landing sites (Table 2) are within 1σ of each other except for MgO and Na_2O, which are the same within 2σ (*26-30*). The MER compositional averages exclude soils that contain a substantial "local component" (high SO_3 and high SiO_2 for Gusev and high Fe_2O_3 for Meridiani). The near identity of compositions of the Rocknest, Gusev, and Meridian basaltic soils implies either global-scale mixing of basaltic material or similar regional-scale basaltic source material or some combination thereof.

In contrast to the APXS measurement at the Portage wheel scuff, both CheMin and SAM measurements were carried out on the sieved, <150 μm size fraction of soil. To discriminate potential differences between the fines delivered to CheMin and SAM and the bulk material analyzed in the wheel scuff, APXS chemistry was obtained from portions of sieved material deposited on the observation tray. APXS spectra from the bulk and sieved material are nearly identical, with the exception of a prominent Ti peak and increased background from the observation tray (reflecting Ti metal of the tray). Additionally, Ca, Mn and Fe signals in spectra from the observation tray are lowered proportionally as a function of their atomic number, suggesting that a fraction of these grains is smaller than the APXS sampling depth (*31*). Slightly elevated S and Cl, with a S/Cl ratio similar to that found in soils by MER (*32*), suggest a potential enrichment of these two elements in the <150 μm fraction delivered to the observation tray.

In order to determine the amount and composition of the amorphous component, mass balance calculations were performed using the chemical composition of the bulk sample, the chemical compositions of the individual phases (plagioclase, sanidine, olivine, etc.) and the relative proportions of those phases in the crystalline component. The empirical formulas of the major crystalline phases (Table 3) and their chemical compositions (Table S2) were calculated from cell parameter data *(20, 21, Table S1).* The chemical formulas and compositions of the minor crystalline components were assigned by stoichiometry (e.g., ilmenite as $TiFeO_3$). The relative proportions of amorphous and crystalline components and their respective bulk compositions are summarized in Table 4, with Rocknest having ~45 wt.% amorphous and ~55 wt.% crystalline components

(33). The chemical compositions and proportions of amorphous and crystalline components were calculated on a light-element-free basis. The relative proportion of the amorphous component will in reality be greater than 45 wt.% because the volatile inventory is associated with that component (*34*).

Abundance estimates for the X-ray amorphous component of a sample may vary considerably depending on the method used for their determination. Bish et al. (20), for example, utilized a full pattern fitting method together with known amorphous standard materials analyzed in the laboratory to determine the amount of amorphous or poorly crystalline material contained in the CheMin X-ray diffraction pattern. Their reported value of ~27 wt. % ± 50 % (1σ range of 13-40 wt %), as calculated from diffraction and scattering data alone, is somewhat lower than the ~45% calculated from mass balance considerations, but both values are within the combined analytical uncertainty of the two techniques.

The inferred chemical composition of the amorphous component (Table 4) contains ~23% "FeO+Fe_2O_3", suggesting that ferric nanophase oxide ("npOx" (*25-26, 35*)) is present in abundance. Similarly, S (principally contained within the amorphous component) is closely associated with the npOx in dunes at the MER sites (*27, 28*) as well. Abundances of SO_3 and Cl are correlated in soils from Gusev and Meridiani, which implies that both are associated with npOx in the amorphous component because these elements are not associated with Mg, Ca, or Fe in crystalline phases. The elements Cr, Mn, and P were associated with the amorphous component (Table 4), but they could

instead be present as crystalline phases (e.g. Ca-phosphate and chromite) at abundances below the CheMin detection limit and/or as substitutional impurities in the major crystalline phases (e.g., Mn and Cr in pyroxene).

The SAM instrument analyzed Rocknest for volatiles species and organic molecules (*34*), and it detected, in order of decreasing abundance: H_2O, SO_2, CO_2, and O_2. The crystalline phases, aside from a minor anhydrite component, do not include these species as a part of their structure, so they must either be present in the amorphous component or be present in the crystalline component at levels below the XRD detection limit, or both.

ChemCam spot observations in the scoop walls of Rocknest are characterized by the strong emissions from elemental hydrogen, although ChemCam is not sensitive to its bonding state (*36*). Comparison of this result with those of CheMin and SAM suggests that ChemCam detections of hydrogen most likely correspond to the H_2O associated with the amorphous component detected by CheMin.

Discussion

Global, regional and local sources

The crystalline phases in the Rocknest fines are consistent with a basaltic source and fit well within the measured qualitative mineralogy of basaltic martian meteorites and the normative mineralogy of Adirondack class olivine basalts at Gusev crater (*25*) (Table 1). If the Rocknest assemblage of basaltic crystalline and amorphous components is locally derived, it is distinct from mafic float rocks analyzed to date by APXS and ChemCam in Gale crater (*36, 37*). This observation suggests that the similarity in the chemical

compositions of aeolian bedforms (basaltic soil) at Gale, Gusev, and Meridiani (Table 2) might result from global-scale aeolian mixing of local-to-regional basaltic material that may or may not have variable chemical compositions. This process would require sufficiently strong winds occurring with sufficient frequency over a long enough time to achieve global or regional-scale transport of grains by saltation and suspension.

An alternative explanation for the comparable chemical compositions of aeolian bedforms at Gale, Gusev, and Meridiani is that the chemical compositions of martian basalts are similar at regional scales everywhere on the planet. The Rocknest sand shadow could reasonably have locally sourced 1-2 mm particles, with finer-grained regional basaltic material plus a contribution from global dust. The similarity of soil compositions (Table 2) suggests that the basaltic fine-grained materials at Gusev, Meridiani and Gale crater provide a reasonable approximation to the bulk composition of the exposed martian crust (*38, 39*).

It is tempting to suggest that the light-toned martian dust is largely represented by the Rocknest amorphous component. However, we have no data to show that the <150 μm size fraction (clay to fine-sand size fraction) of material analyzed by CheMin has its finest material preferentially enriched in amorphous material. The evidence from MER for basaltic soils suggests that the chemical composition of the fine-grained, light-toned soil is approximately the same as the coarser-grained, dark-toned soils (e.g., Table 10 of (*40*)).

The central mound of Gale crater (Mt. Sharp or Aeolis Mons) exhibits reflectance spectra suggesting the presence of crystalline hydrated sulfate minerals and

phyllosilicates (*41*), but neither was seen in Rocknest (above the 1-2% level). The absence of material from Mt. Sharp could arise from the wind pattern during formation of the Rocknest sand shadow – it is oriented so as to imply sediment transport from the north, and Mt. Sharp is east and southeast of Rocknest.

Materials and Methods

Calculation of windspeeds required to form the Rocknest sand shadow

The wind velocity required to move the coarse grains of the sand shadow by creep can be calculated. The critical shear velocity (u_{*c}) of the wind needed to transport 1 mm grains (d) is given by (*44*) as

$$u_{*c} = \sqrt{0.0123 \left(sgd + \frac{0.0003\ kg/s^2}{\rho_f d}\right)},$$

where $s = \rho_s/\rho_f$, ρ_s is the density of the grains using basalt (3000 kg/m^3), ρ_f is the density of martian air (0.02 kg/m^3), and g is the acceleration due to gravity (3.71 m/s^2). The calculated u_{*C} is 2.6 m/s, which represents the fluid shear velocity to initiate motion. Because grains in creep derive a portion of their momentum from collisions by saltating grains, on Earth once saltation begins creep can occur down to 0.7 u_{*c} (1.8 m/s as applied to the Rocknest grains), which represents the impact threshold for motion. Given a boundary layer created by winds blowing over the surface, shear velocities can then be related to the wind speeds above the surface by the law-of-the-wall

$$u_z = \frac{u_*}{k} \ln\left(\frac{z}{z_o}\right),$$

where u_z is the wind speed at height z above the surface (taken here as 1 m), k is a constant of 0.407, and z_o is the roughness height where the idealized logarithmic wind

profile is predicted to be zero. Roughness height varies by grain size and the height of surface features such as wind ripples (*7*), and also by the height and intensity of the saltation cloud (*45*). Rocknest conditions are unknown, but z_0 is taken as 0.3 mm, which would be the roughness height with wind ripples 10 mm in height. Estimated wind speeds at 1 m above the surface are ~ 52 m/s (116 mph) and 36 m/s (80 mph) without and with saltation, respectively. As a result of the lower gravity and reduced atmospheric density on Mars, a greater hysteresis exists than on Earth between the fluid and impact thresholds, and saltation impacts upon grains are more energetic (*18, 46-47*). The combined effects suggest that initial transport of the coarse surface grains probably occurred at lower wind speeds than those calculated. Conversely, reactivation of the sand shadow would require significantly higher wind speeds because of induration of the surface.

Although observations from the Viking Lander 1 suggest that wind speeds of 30 m/s at a height of 1.6 m occurred during its two year lifetime (*48*), we do not known how often Mars winds can be capable of transporting 1-2 mm grains. The wind estimates above suggest that formation of the Rocknest sand shadow has involved rare strong winds, and that re-activation of the sand shadow from its currently indurated state would require even stronger and rarer winds.

Given the possibility of significant antiquity of the Rocknest sand shadow and similar coarse-grained bedforms on Mars, could their activation correspond to the martian obliquity cycle? At low obliquities the atmosphere collapses onto the polar caps, but at

high obliquity CO_2 is released to the atmosphere (*49, 50*). Taken as an end-member, atmospheric density may double at high obliquity and thereby enhance aeolian activity (*50*). As a comparison with the above values calculated for the present martian atmosphere, using 0.04 kg/m^3 for atmospheric density, the calculated fluid u_{*c} is 1.9 m/s and the impact u_{*c} is 1.3 m/s, which correspond to wind speeds at the 1 m height of ~ 37 m/s (83 mph) and 26 m/s (58 mph), respectively. Although significantly lower than values calculated for present conditions, rare strong wind events are still implied.

References and Notes

(1) A Mars solar day has a mean period of 24 hours, 39 minutes 35 seconds, and is customarily referred to as a "sol" to distinguish it from the roughly 3% shorter day on Earth.

(2) A sand shadow is an accumulation of wind-blown sediment deposited in the lower-velocity lee of an obstacle in the path of the wind.

(*3*) R.C. Anderson, L. Jandura, A.B. Okon, D. Sunshine, C. Roumeliotis, et al., Collecting Samples in Gale Crater, Mars; An Overview of the Mars Science Laboratory Sample Acquisition, Sample Processing and Handling System. *Space Sci. Rev.* **170**:57-76, DOI 10.1007/s11214-012-9905-1 (2012).

(*4*) M.S. Anderson, I. Katz, M. Petkov, B. Blakkolb, J. Mennella et al., In situ cleaning of instruments for the sensitive detection of organics on Mars. *Rev. Sci. Instr.,* 83:10 105109 DOI: 10.1063/1.4757861 (2012).

(*5*) D.F. Blake, D. Vaniman, C. Achilles, R. Anderson, D. Bish et al., Characterization and Calibration of the CheMin Mineralogical Instrument on Mars Science Laboratory. *Space Sci Rev* **170**:341-478, DOI 10.1007/s11214-012-9905-1 (2012).

(*6*) P.R. Mahaffy, C.R. Webster, M. Cabane, P.G. Conrad, P. Coll et al., The Sample Analysis at Mars Investigation and Instrument Suite. *Space Sci Rev* **170**:401-399, DOI 10.1007/s11214-012-9905-1 (2012).

(*7*) R.A. Bagnold, The Physics of Blown Sand and Desert Dunes. Chapman and Hall (London) 265 pp (1941).

(*8*) K.S. Edgett, R. A. Yingst, M.A. Ravine, M.A. Caplinger, J.N. Maki, et al., Curiosity's Mars Hand Lens Imager (MAHLI) Investigation. *Space Sci Rev* **170**:259-318, DOI 10.1007/s11214-012-9905-1 (2012).

(*9*) W. Goetz, W.T. Pike, S.F. Hviid, M.B. Madsen, R.V. Morris et al., Microscopic analysis of soils at the Phoenix landing site, Mars: Classification of soil particles and description of their optical and magnetic properties. *J. Geophys. Res.,* **115**, E00E22, doi:10.1029/2009JE003437 (2010).

(*10*) K.E. Herkenhoff, M.P. Golombek, E.A. Guinness, J.B. Johnson, A. Kusack, *et al*., In situ observations of the physical properties of the martian surface. IN The Martian Surface: Composition, Mineralogy, and Physical Properties, ed. J.F. Bell III, Cambridge University Press (Cambridge) 451-467 (2008).

(*11*) R. Sullivan, R. Arvidson, J.F. Bell III, R.Gellert, M. Golombek, *et al*., Wind-driven particle mobility on Mars: Insights from Mars Exploration Rover observations at "El Dorado" and surroundings at Gusev Crater. *J. Geophys. Res.* **113**, E06S07, doi:10.1029/2008JE003101 (2008).

(*12*) L.A. Soderblom, R.C. Anderson, R.E. Arvidson, J.F. Bell III, N.A. Cabrol, *et al*., Soils of Eagle crater and Meridiani Planum at the Opportunity rover landing site. *Science* **306**, 1723-1726 (2004).

(*13*) R. Sullivan, D. Banfield, J.F. Bell III, W. Calvin, D. Fike, *et al*., Aeolian processes at the Mars exploration rover Meridiani Planum landing site. *Nature* **436**, 58-61 (2005).

(*14*) S.G. Fryberger, P. Hesp and K. Hastings, Aeolian granule ripple deposits, Namibia. *Sedimentology* **39**, 319-331 (1992).

(*15*) D.J. Jerolmack, D. Mohrig, J.P. Grotzinger, D.A. Fike and W.A. Watters, Spatial grain size sorting in eolian ripples and estimation of wind conditions on planetary surfaces: application to Meridiani Planum, Mars. *J. Geophys. Res.* **111**, E12S02, doi:10.1029/2005JE002544 (2006).

(*16*) J.M. Ellwood, P.D. Evans and I.G. Wilson, Small scale aeolian bedforms. *J. Sed. Petrol.***45**, 554-561 (1975).

(*17*) P.A. Hesp, The formation of shadow dunes. *J. Sed. Petrol*. **51**, 101-112.

(*18*) M.P. Almeida, E.J.R. Parteli, J.S. Andrade and H.J. Herrmann, Giant saltation on Mars. *Proceed. Nat. Acad. Sci.* **105**, 6222-6226 (2008).

(*19*) M.P. Golombek, K. Robinson, A. McEwen, N. Bridges, B. Ivanov, *et al.,* Constraints on ripple migration at Meridiani Planum from Opportunity and HiRISE observations of fresh craters. *J. Geophys. Res.* **115**, E00F08, doi:10.10292010JE003628 (2010).

(*20*) D.L. Bish, D.F. Blake, D.T. Vaniman, S.J. Chipera, R.V. Morris, et al., X-ray Diffraction Results from Mars Science Laboratory: Mineralogy of Rocknest Aeolian Bedform at Gale Crater. Science, **submitted** (2013)

(21) Supplementary materials are available on *Science* Online.

(*22*) Unit cell parameters obtained from the RRUFF Project database: http://rruff.info/ima.

(*23*) S.R. Taylor and S.M. McLennan, Planetary Crusts: Their Composition, Origin and Evolution. Cambridge University Press (Cambridge) 378 pp (2009).

(*24*) R.V. Morris, G. Klingelhöfer, C. Schröeder, I. Fleisher, D.W. Ming et al., Iron mineralogy and aqueous alteration from Husband Hill through Home Plate at Gusev Crater, Mars: Results from the Mössbauer instrument on the Spirit Mars Exploration Rover. *J. Geophys. Res.* **113**, E12S39, doi:10.1029/2008JE003201 (2008).

(*25*) D.W. Ming, R. Gellert, R.V. Morris, R.E. Arvidson, J. Bruckner et al., Geochemical properties of rocks and soils in Gusev Crater, Mars: Results of the Alpha Particle X-ray Spectrometer from Cumberland Ridge to Home Plate. *J. Geophys. Res.* **113**, E12S39, doi:10.1029/2008JE003195 (2008).

(*26*) R. V. Morris, G. Klingelhöfer, C. Schröder, D. S. Rodionov, A. Yen, *et al.*, Mössbauer mineralogy of rock, soil, and dust at Gusev Crater, Mars: Spirit's journey through weakly altered olivine basalt on the Plains and pervasively altered basalt in the Columbia Hills. *J. Geophys. Res.* **111**, E02S13, doi:10.1029/2006JE002791 (2006).

(*27*) R.V. Morris, G. Klingelhöfer, C. Schröeder, I. Fleisher, D.W. Ming et al., Iron mineralogy and aqueous alteration from Husband Hill through Home Plate at Gusev Crater, Mars: Results from the Mössbauer instrument on the Spirit Mars Exploration Rover. *J. Geophys. Res.* **113**, E12S39, doi:10.1029/2008JE003201 (2008).

(*28*) A. S. Yen, R. Gellert, C. Schroder, R. V. Morris, J. F. Bell, *et al.,* An integrated view of the chemistry and mineralogy of martian soils. *Nature* **436**, 49-54, doi:10.1038.nature03637 (2005).

(*29*) D.W. Ming, R. Gellert, R.V. Morris, R.E. Arvidson, J. Bruckner et al., Geochemical properties of rocks and soils in Gusev Crater, Mars: Results of the Alpha Particle X-ray Spectrometer from Cumberland Ridge to Home Plate. *J. Geophys. Res.* **113**, E12S39, doi:10.1029/2008JE003195 (2008).

(*30*) A. S. Yen, R. Gellert, B. C. Clark, D. W. Ming, P. L. King, *et al.*, Evidence for a global martian soil composition extends to Gale crater. *45th Lunar and Planetary Science Conference*, March, 2013, Published on CD by the Lunar and Planetary Institute, Houston, Texas Abstr.# 2495 (2013).

(*31*) J.A. Berger, P.L. King, R. Gellert, J.L. Campbell, N. Boyd et al., MSL Titanium Observation Tray Measurements with APXS. *45th Lunar and Planetary Science Conference*, March, 2013, Published on CD by the Lunar and Planetary Institute, Houston, Texas abstract #1321 (2013).

(*32*) R. Gellert, et al., Alpha Particle X-ray Spectrometer (APXS): Results from Gusev Crater and calibration report. *J. Geophys. Res.* **111**, E02S05, doi:10/1029/2005JE002555 (2006).

(33) Because APXS does not discriminate among iron oxidation states, the total Fe concentration was proportioned in accordance with the oxidation state information carried by the crystalline phases (Table 3, column 3). FeO-Cryst and Fe_2O_3-Cryst are the concentrations of FeO and Fe_2O_3 required to accommodate olivine, augite, pigeonite, ilmenite, and magnetite and hematite, in accordance with their valence states. The remaining iron (FeO + Fe_2O_3) is then associated with the amorphous component without implications for oxidation state. Similarly, some SO_3 is reported as SO_3-Cryst to accommodate anhydrite as a crystalline component.

(*34*) L. A. Leshin, P. Mahaffy, C. Webster, M. Cabane, P. Coll, *et al.,* Insights into Martian Fines from Volatile, Isotope and Organic Analysis with the Mars Curiosity Rover. *Science* **submitted** (2013).

(*35*) Nanophase ferric oxide (npOx) is a generic name for amorphous, poorly crystalline, or short-range ordered products of oxidative alteration/weathering that have octahedrally coordinated Fe^{3+} (Mössbauer doublet) and are predominantly oxide/oxyhydroxide/hydrous in nature. Depending on local conditions, npOx (as encountered on the Earth) can be any combination of superparamagnetic hematite and goethite, lepidocrocite, ferrihydrite, schwertmannite, akaganeite, hisingerite, and the octahedral Fe^{3+}-rich particles that pigment iddingsite and palagonite. NpOx can also incorporate anions like $(SO_4)^{2-}$, Cl^- and $(PO_4)^{3-}$ through specific chemical adsorption. Because of different local conditions on Mars, one or more forms of npOx on the planet may be uncommon or not present on Earth.

(*36*) P. –Y. Meslin, O. Gasnault, O. Forni, S. Schroder, S. Clegg et al., Soil diversity and hydration as observed by ChemCam at Gale crater, Mars. *Science*, **submitted** (2013).

(37) R. Gellert, J.A. Berger, N. Boyd, C. Brunet, J.L. Campbell, et al., Initial MSL APXS activities and observations at Gale crater, Mars. *45th Lunar and Planetary Science Conference*, March, 2013, Published on CD by the Lunar and Planetary Institute, Houston, Texas, abstract #1432 (2013).

(*38*) H.Y. McSween, G. J. Taylor, and M. B. Wyatt, Elemental composition of the Martian crust. *Science*, **324**, 736-739 (2009).

(*39*) S.R. Taylor and S.M. McLennan, Planetary Crusts: Their Composition, Origin and Evolution. Cambridge Univ. Press (Cambridge) 378pp. (2009).

(*40*) R. V. Morris, G. Klingelhöfer, C. Schröder, D. S. Rodionov, A. Yen, *et al.*, Mössbauer mineralogy of rock, soil, and dust at Meridiani Planum, Mars: Opportunity's journey across sulgate-rich outcrop, basaltic sand and dust, and hematite lag deposits. *J. Geophys. Res.* **111**, E02S13, doi:10.1029/2006JE002791 (2006).

(41) Milliken, R.E, et al., (2010) GRL 37, L04201, doi: 10.1029/2009GL041870, 2010

(*42*) D.H. Lindsley, Pyroxene thermometry. *American Mineralogist* 68, 477-493 (1983).

(*43*) P.H. Warren and J.T. Wasson, The compositional-petrographic search for pristine nonmare rocks: Third foray. *Proc. Lunar Planet. Sci. Conf. 10th,* 583-610 (1979).

(*44*) Y. Shao and H. Lu, A simple expression for wind erosion threshold friction velocity. *J. Geophys. Res.* **105**, 22,437-22,443 (2000).

(*45*) P.R. Owen, P.R., Saltation of uniform grains in air. *J. Fluid Mech*. **20**, 225-242 (1964).

(*46*) P. Claudin and B. Andreotti, A scaling law for aeolian dunes on Mars, Venus, Earth, and for subaqueous ripples. *Earth Planet. Sci. Lett.* **252**, 30-44 (2006).

(*47*) J.F. Kok, Difference in the wind speeds required for initiation versus continuation of sand transport on Mars: Implications for dunes and dust storms. *Phys. Rev. Lett* **104**, doi:10.1103/PRL.104.074502 (2010).

(*48*) R.E. Arvidson, E.A. Guinness, H.J. Moore, J. Tillman and S.D. Wall, Three Mars years: Viking Lander 1 imaging observations. Science **222**, 463-468 (1983).

(*49*) C.E. Newman, S.R. Lewis and P.L. Read, The atmospheric circulation and dust activity in different orbital epochs on Mars. *Icarus* **174**, 135-160 (2005)

(*50*) R. J. Phillips, B.J. Davis, K.L. Tanaka, S. Byrne, M.T. Mellon, *et al.*, Massive CO_2 ice deposits sequestered in the south polar layered deposits of Mars. *Science* **332**, 838-841 (2011).

Support from the NASA Mars Science Laboratory Mission is gratefully acknowledged. The chemical and mineralogical data presented here are derived from the archived data sets in the NASA Planetary Data System (PDS) http://pds-geosciences.wustl.edu/missions/msl/, specifically MSL-M-CHEMIN-2-EDR-V1.0 and MSL-M-APXS-2-EDR-V1.0. MBM was funded by the Danish Council for Independent Research/Natural Sciences (FNU grants 12-127126 and 11-107019). WG acknowledges partial funding by the Deutsche Forschungsgemeinschaft (DFG grant GO 2288/1-1). Some of this research was carried out at Jet Propulsion Laboratory, California Institute of Technology under a contract with the National Aeronautics and Space Administration.

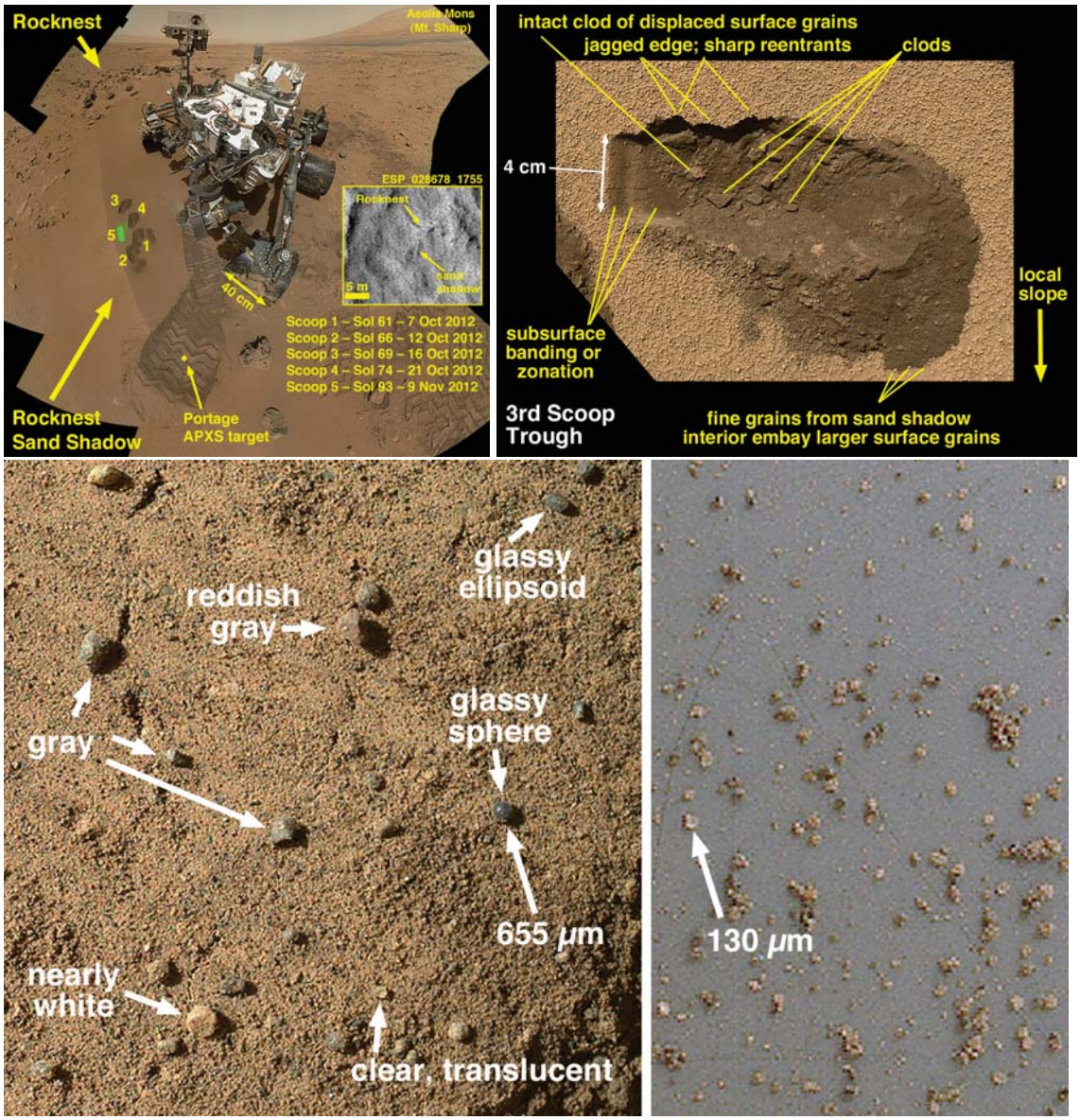

Figure 1. The Rocknest sand shadow, where *Curiosity* spent Sols 57-100 conducting engineering tests and science observations of the material. **(A)** (upper left) Mosaic of 55 MAHLI images showing Curiosity parked on the east side of the Rocknest sand shadow during the sampling campaign on Sol 84. The location of each of the five scoops is indicated. The inset is a portion of MRO HiRISE image ESP_028678_1755 showing the Rocknest sand shadow as seen from about 282 km above the ground. **(B)** (upper right) MAHLI image of third scoop trench, showing the dust-coated, indurated, armoring layer of coarse and very coarse sand and underlying, darker, fine and very find sand. **(C)** (lower left) MAHLI image of Rocknest sand shadow surface disrupted by the rover's front, left wheel on Sol 57. The larger grains came from the armoring layer of coarse sand on the sand shadow surface. **(D)** (lower right), MAHLI image of a <150 μm sieved portion from the third scoop; grains similar to those delivered to the CheMin and SAM instruments, delivered to Curiosity's Ti observation tray.

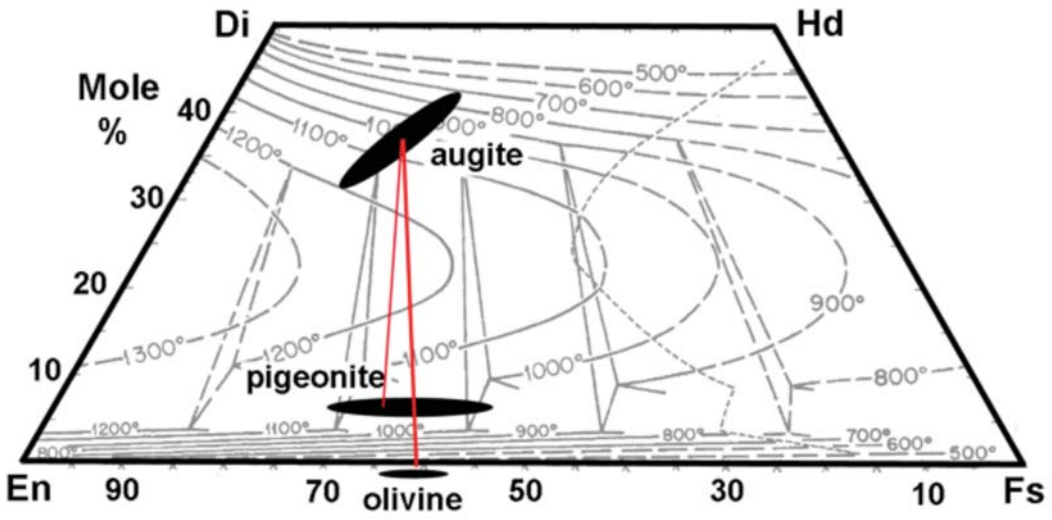

Figure 2. Pyroxene compositional quadrilateral, showing the chemical and thermal relationship between the major igneous minerals in the Rocknest sand shadow. Compositions of augite, pigeonite, and olivine in the Rocknest dune material, plotted on the pyroxene quadrilateral: En, enstatite, $Mg_2Si_2O_6$; Di, diopside, $CaMgSi_2O_6$; Hd, hedenbergite, $CaFeSi_2O_6$; and Fs, ferrosilite, $Fe_2Si_2O_6$. Pyroxenes are plotted within the quadrangle, based on CheMin XRD unit-cell parameters; olivine is plotted below the quadrilateral at the appropriate molar Mg/Fe ratio (*20*). Ellipses for each mineral approximate the uncertainties in mineral compositions from their unit-cell parameters. Gray background lines represent the surface of the pyroxene solvus, with temperatures in °C (*42*). Red lines are approximate equilibrium tie lines from the augite centroid composition to compositions of olivine and pigeonite, based on similar tie lines in an equilibrated anorthosite in lunar sample 62236 (*43*).

Table 1. Mineralogy of Rocknest soil (CheMin XRD) and normative mineralogies of basaltic materials from Gusev crater and of martian meteorites (Rocknest data are amorphous-free values).

Location	Gale	Gusev			Meteorites			
Sample	Rocknest Sand Shadow	Adirondack	Backstay	Irvine	Shergotty	NWA 6234	EETA 79001A	QUE 94210
Quartz	*1.4*	0	0	0	0.2	0	0	3
Plagioclase	40.8	39	49	32	23	19	19	32
K-spar	*1.3*	1	6	6	1	0.5	0	0
Low-Ca Pyx	13.9	15	14	21	46	30	47	15
High-Ca Pyx	14.6	15	5	13	25	16	16	38
Olivine	22.4	20	15	16	0	27	13	0
Fe-Cr oxides	*3.2*	6	4	6	3	4	2	0
Ilmenite	*0.9*	1	2	2	2	2	1	4
Apatite	-	1	3	2	2	2	1	6
Anhydrite	*1.5*							
Mg#	61±3	57	62	55	51	63	63	40
An	57±3	42	29	19	51	50	60	62

Notes for Table 1: Rocknest soil by CheMin (*20*), average of scoop 5, proportions of crystalline phases normalized to 100%; values in italics uncertain. CIPW norms (weight) for Gusev basaltic materials from MER APXS chemical analyses (*26*) ignoring S and Cl; Fe^{3+}/Fe_{tot} for Backstay and Irvine taken as 0.17, the value for RATted Adirondack basalt (*26*). CIPW norms (weight %) of martian meteorites from bulk compositions [t-x]; Fe^{3+}/Fe_{tot} as analyzed, and estimated at 0.1 for NWA 6234 and 0 for QUE94201. 'K-spar' is sanidine for the Rocknest soil, and normative orthoclase for others. 'Low-Ca Pyx' is pigeonite for the soil, and normative hypersthene for others. 'High-Ca Pyx' is augite for the soil, and normative diopside for others. 'Fe-Cr oxide' includes magnetite, hematite and chromite. All phosphorus in analyses calculated as normative apatite.

Table 2. Basaltic soil compositions from APXS analyses for Rocknest_Portage, Gusev Crater, and Meridiani Planum

	Rocknest	Gusev	Meridiani
Number	1[a]	48[b]	29[b]
SiO_2 (wt.%)	42.88 ± 0.47	46.1 ± 0.9	45.7 ± 1.3
TiO_2	1.19 ± 0.03	0.88 ± 0.19	1.03 ± 0.12
Al_2O_3	9.43 ± 0.14	10.19 ± 0.69	9.25 ± 0.50
Cr_2O_3	0.49 ± 0.02	0.33 ± 0.07	0.41 ± 0.06
Fe_2O_3 + FeO	19.19 ± 0.12	16.3 ± 1.1	18.8 ± 1.2
MnO	0.41 ± 0.01	0.32 ± 0.03	0.37 ± 0.02
MgO	8.69 ± 0.14	8.67 ± 0.60	7.38 ± 0.29
CaO	7.28 ± 0.07	6.3 ± 0.29	6.93 ± 0.32
Na_2O	2.72 ± 0.10	3.01 ± 0.30	2.21 ± 0.18
K_2O	0.49 ± 0.01	0.44 ± 0.07	0.48 ± 0.05
P_2O_5	0.94 ± 0.03	0.91 ± 0.31	0.84 ± 0.06
SO_3	5.45 ± 0.10	5.78 ± 1.25	5.83 ± 1.04
Cl	0.69 ± 0.02	0.7 ± 0.16	0.65 ± 0.09
Br (μg/g)	26 ± 6	53 ± 46	100 ± 111
Ni	446 ± 29	476 ± 142	457 ± 97
Zn	337 ± 17	270 ± 90	309 ± 87
Sum (wt.%)	99.85	99.88	99.88
Cl/SO_3	0.13 ± 0.02	0.12 ± 0.02	0.11 ± 0.01

[a]Gellert et al., 2013 *(37)*; analytical uncertainty.

[b]1-σ standard deviation of average.

Table 3. Empirical chemical formulas of the four major phases identified in the Rocknest soil estimated by crystal-chemical techniques.

olivine	$(Mg_{0.62(3)}Fe_{0.38})_2SiO_4$
plagioclase	$(Ca_{0.57(13)}Na_{0.43})(Al_{1.57}Si_{2.43})O_8$
augite	$(Ca_{0.75(4)}Mg_{0.88(10)}Fe_{0.37})Si_2O_6$
pigeonite	$(Mg_{1.13(9)}Fe_{0.68(10)}Ca_{0.19})Si_2O_6$

Table 4. Chemical composition and proportion of XRD amorphous component in Rocknest_Portage from APXS and CheMin data.

	Origin		Remove XRD Crystalline Compoment[1]										Composition	
	APXS[2]	APXS+ CheMin	Plagio-clase	San-idine	Olivine	Augite	Pige-onite	Ilm-enite	Hem-atite	Mag-netite	Anhyd-rite	Quartz	Amor-phous[3]	Crysta-lline
SiO_2, wt. %	42.88	42.88	30.88	30.42	25.95	21.63	17.51	17.51	17.51	17.51	17.51	16.76	37.20	47.59
TiO_2	1.19	1.19	1.19	1.19	1.19	1.19	1.19	0.93	0.93	0.93	0.93	0.93	2.06	0.47
Al_2O_3	9.43	9.43	2.85	2.72	2.72	2.72	2.72	2.72	2.72	2.72	2.72	2.72	6.04	12.24
Cr_2O_3	0.49	0.49	0.49	0.49	0.49	0.49	0.49	0.49	0.49	0.49	0.49	0.49	1.09	0.00
$FeO+Fe_2O_3$[4]	19.19	10.43	10.43	10.43	10.43	10.43	10.43	10.43	10.43	10.43	10.43	10.43	23.14	-0.10
FeO-Cryst[5]	---	7.37	7.37	7.37	3.31	2.29	0.59	0.35	0.35	0.00	0.00	0.00	-0.01	13.48
Fe_2O_3-Cryst[6]	---	1.39	1.39	1.39	1.39	1.39	1.39	1.39	0.79	0.00	0.00	0.00	-0.01	2.55
MnO	0.41	0.41	0.41	0.41	0.41	0.41	0.41	0.41	0.41	0.41	0.41	0.41	0.91	0.00
MgO	8.69	8.69	8.69	8.69	4.97	3.72	2.19	2.19	2.19	2.19	2.19	2.19	4.86	11.86
CaO	7.28	7.28	4.65	4.65	4.65	3.19	2.87	2.87	2.87	2.87	2.53	2.53	5.61	8.67
Na_2O	2.72	2.72	1.62	1.60	1.60	1.60	1.60	1.60	1.60	1.60	1.60	1.60	3.56	2.03
K_2O	0.49	0.49	0.49	0.40	0.40	0.40	0.40	0.40	0.40	0.40	0.40	0.40	0.89	0.16
P_2O_5	0.94	0.94	0.94	0.94	0.94	0.94	0.94	0.94	0.94	0.94	0.94	0.94	2.09	-0.01
SO_3	5.45	4.96	4.96	4.96	4.96	4.96	4.96	4.96	4.96	4.96	4.96	4.96	11.01	-0.05
SO_3-Cryst[7]	---	0.49	0.49	0.49	0.49	0.49	0.49	0.49	0.49	0.49	0.00	0.00	-0.01	0.90
Cl	0.61	0.61	0.61	0.61	0.61	0.61	0.61	0.61	0.61	0.61	0.61	0.61	1.35	-0.01
Sum	99.77	99.77	77.47	76.77	64.52	56.47	48.80	48.30	47.70	46.55	45.71	44.96	99.77	99.77
$\sum(FeO+Fe_2O_3)$	19.19	19.19	---	---	---	---	---	---	---	---	---	---	23.14	16.03
$\sum(SO_3)$	5.54	5.54	---	---	---	---	---	---	---	---	---	---	11.01	0.90
Relative to Whole Sample			22.3	0.7	12.3	8.0	7.6	0.5	0.6	1.2	0.8	0.8	**45.3**	**54.7**
Relative to XRD Crystalline			40.8	1.3	22.4	14.6	13.9	0.9	1.1	2.1	1.5	1.4	---	100.0

1. Plagioclase = An57; olivine = Fo62; Augite = En44Fs20Wo36 (Mg/Fe = 2.2 atomic); Pigeonite = En56Fs35Wo8 (Fe/Mg = 1.6 atomic).
2. APXS chemistry from Gellert et al. (37).
3. Cr_2O_3 and MnO calculated with the amorphous component.
4. Total Fe as $FeO+Fe_2O_3$ because APXS does not distinguish oxidation states.
5. FeO required for Fe^{2+} crystalline phases (olivine, augite, pigeonite, ilmenite, and magnetite).
6. Fe_2O_3 required for Fe^{3+} crystalline phases (hematite and magnetite).
7. SO_3 required for crystalline SO_3 crystalline phase (anhydrite).

Supplementary Materials for

CURIOSITY AT GALE CRATER, MARS: CHARACTERIZATION AND ANALYSIS OF THE ROCKNEST SAND SHADOW

D. F. Blake[1]*, R. V. Morris[2], G. Kocurek[3], S. M. Morrison[4], R. T. Downs[4], D. Bish[5], D. W. Ming[2], K. S. Edgett[6], D. Rubin[7], W. Goetz[8], M. B. Madsen[9], R. Sullivan[10], R. Gellert[11], I. Campbell[11], A. H. Treiman[12], S.M. McLennan[13], A. S. Yen[14], J. Grotzinger[15], D. T. Vaniman[16], S. J. Chipera[17], C. N. Achilles[2], E. B. Rampe[2], D. Sumner[18], P-Y Meslin[19], S. Maurice[19], O. Forni[19], O. Gasnault[19], M. Fisk[20], M. Schmidt[21], P. Mahaffy[22], L. A. Leshin[23], D. Glavin[22], A. Steele[24], C. Freissinet[22], R. Navarro-González[25], R. A. Yingst[16], L. C. Kah[26], N. Bridges[27], K. W. Lewis[28],T. F. Bristow[1], J. D. Farmer[29], J. A. Crisp[14], E. M. Stolper[15], D. J. Des Marais[1], P. Sarrazin[30] and the MSL Science Team[31]

correspondence to: david.blake@nasa.gov

This PDF file includes:

Supplementary Text

Calculation of mineral compositions from their unit-cell parameters

The chemical compositions of the major mineral phases found in the Rocknest sediment fines were determined by relating their refined unit-cell parameters (Table S1, from (*20*)) to those published in the literature (*22*). The figures below show the unit-cell parameter versus chemical composition plots used to estimate the elemental compositions of olivine, plagioclase, augite and pigeonite (Table 3) and their empirical chemical formulas (Table S2).

Table S1.

Wt. % and refined unit-cell parameters of the major crystalline phases in Rocknest (20).

Mineral	Wt.%	2σ	*a* (Å)	*b* (Å)	*c* (Å)	α (°)	β (°)	γ (°)
plagioclase	40.8%	2.4%	8.177(6)	12.868(9)	7.113(5)	93.43(4)	116.26(2)	90.13(3)
forsterite	22.4%	1.9%	10.327(7)	6.034(7)	4.771(5)	90	90	90
augite	14.6%	2.8%	9.782(9)	8.939(9)	5.269(7)	90	106.25(9)	90
pigeonite	13.8%	2.8%	9.652(9)	8.92(1)	5.254(7)	90	108.0(1)	90

Olivine

The Mg-content of olivine was obtained from the variation of Mg-content versus the unit-cell volume using data from the fayalite-forsterite join (Fig. S1). The least-squares equation for the number of atoms of Mg per formula unit (Mg#) as a function of the unit-cell volume is:

$$Mg\# = -0.0578V + 17.801$$

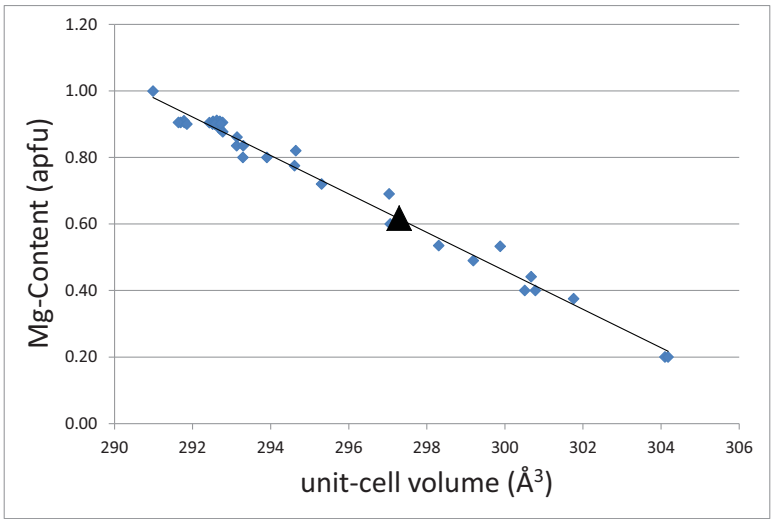

Fig. S1.
Mg-content of Fa-Fo olivine as a function of unit-cell volume. The black triangle represents the Rocknest olivine, indicating a composition of Fo 62.

Plagioclase

The refined unit-cell parameters provided information on the composition of plagioclase feldspar along the Ca-Na join. High-Ca feldspars are characterized by a *c* unit-cell parameter that is double that of lower-Ca feldspars; therefore, our data were restricted to the lower-Ca feldspars. Variations in Ca-content with unit-cell parameters are given in Fig. S2a, S2b and S2c. Fig. S2a shows that the *b* unit-cell parameter is not suitable for determining composition; therefore *c* and α were selected to determine the chemistry.

$Ca\# = 157.0882779c^2 - 2251.2412721c + 8065.692$ (Fig. S2b)
$Ca\# = 0.6896416\alpha^2 - 130.2226916\alpha + 6147.38751$ (Fig. S2c)

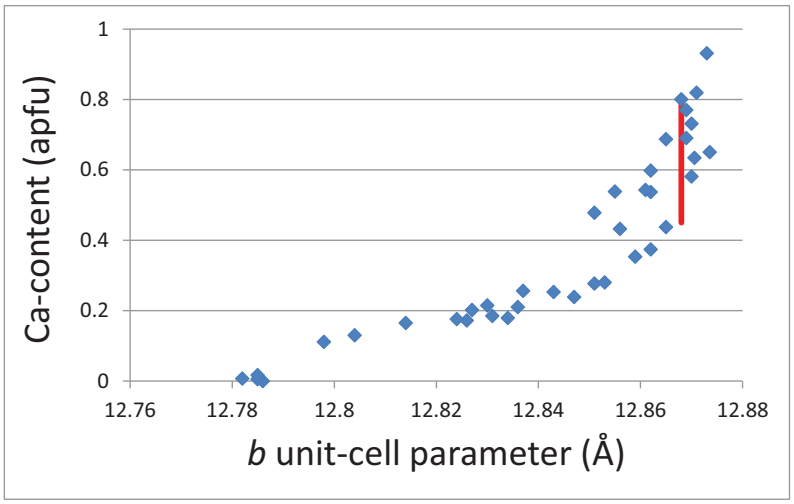

Fig. S2a

Ca-content of K-free plagioclase as a function of the *b* unit-cell parameter. The large scatter of data provides an error estimate of 12%.

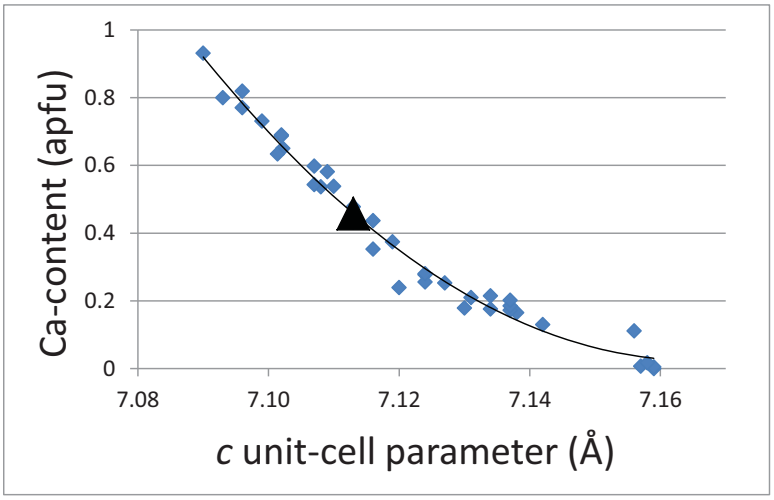

Fig. S2b

Ca-content of K-free plagioclase as a function of the *c* unit-cell parameter. This trend provides a lower bound on the amount of Ca (black triangle denotes Rocknest data).

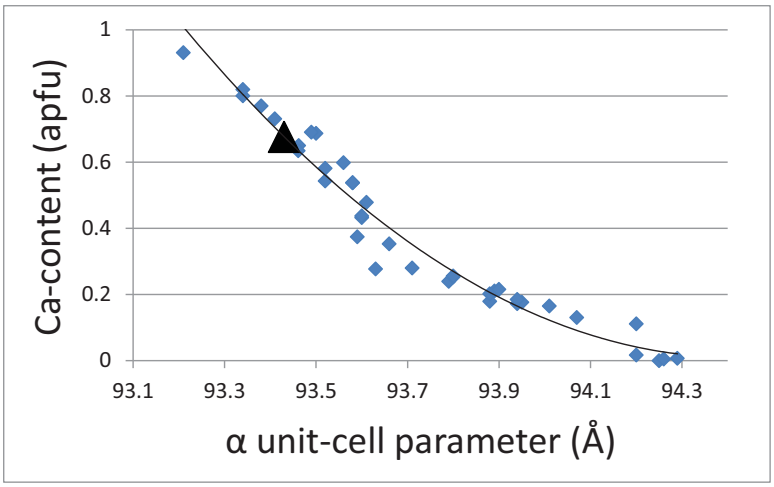

Fig. S2c

Ca-content of K-free plagioclase as a function of the α unit-cell parameter. This trend provides an upper bound on the amount of Ca (black triangle represents the Rocknest plagioclase).

Augite

Mg-content can be obtained from the variation of the *b* unit-cell parameter (Fig. S3a).

Mg# = -9.8029b + 88.509

Fe/Mg content as a function of β has two sets of well-determined trends, that of Ca# = 1.0 and Ca# = 0.8 (Fig. S3b). Regressions of Mg-content for these two trends are:

Mg# = 0.9157β - 95.956 (Ca# = 1.0)
Mg# = 1.3719β - 144.74 (Ca# = 0.8)

Substituting the value of Mg# determined from *b* produced β equal to 105.761° for the Ca# = 1.0 trend and β equal to 106.145° for the Ca# = 0.8 trend. Linear interpolation, using our value of β, gives Ca# = 0.75. The value for Fe# = 2 - Mg# - Ca#.

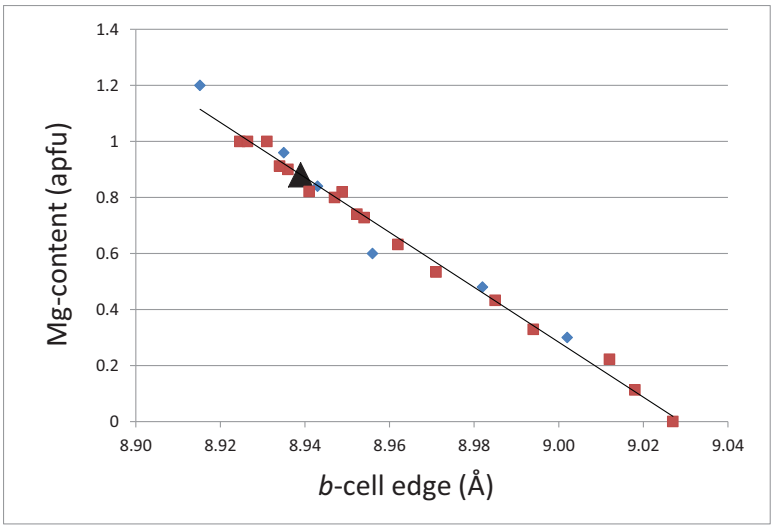

Fig. S3a

Variation of Mg-content with *b* unit-cell parameter in augite. Blue diamonds represent samples with Ca# = 0.8 and red squares are Ca# = 1. The black triangle represents the Rocknest augite – corresponding to a Mg# of 0.88.

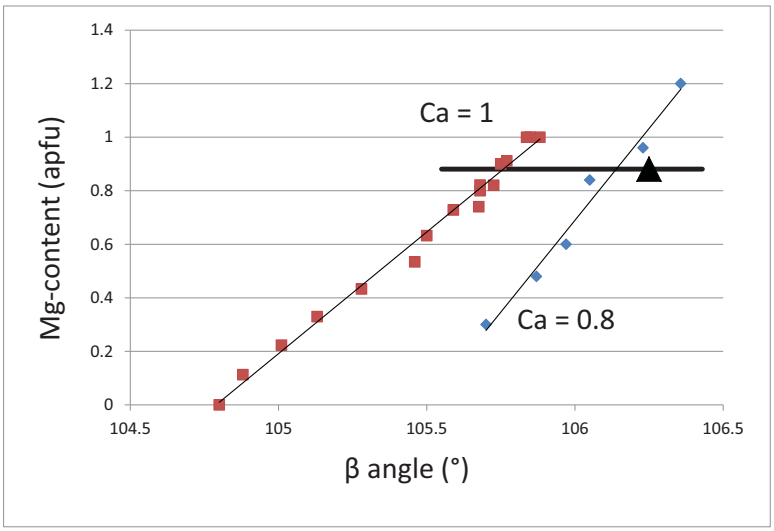

Fig. S3b

Ca-content in augite obtained by scaling the separation between the two trends of Mg-content versus β angle at Ca# = 1 (red squares) and Ca# = 0.8 (blue diamonds). The black triangle represents the Rocknest augite Mg-content at the refined β angle and corresponds to Ca# = 0.75.

Pigeonite

The Mg-content of pigeonite can be obtained from the *b* unit-cell parameter (Fig. S4a).

Mg# = -8.9762*b* + 81.195

The Mg-Ca content as a function of unit-cell volume, V, has two sets of well-developed trends, that of Fe# = 1 and Fe# = 0 (Fig. S4b). Regressions of Mg-content for these two trends are:

Mg# = -0.0471V + 21.148 (Fe# = 1)
Mg# = -0.0254V + 12.572 (Fe# = 0)

Substituting the refined unit-cell volume from the Rocknest pigeonite gave Mg# = 0.89 for the Fe# = 1 trend and Mg# = 1.65 for the Fe# = 0 trend. Linear interpolation, using the Rocknest pigeonite Mg# estimated from *b* (1.13), gives Fe# = 0.68. The values for Ca# = 2 - Mg# - Fe#.

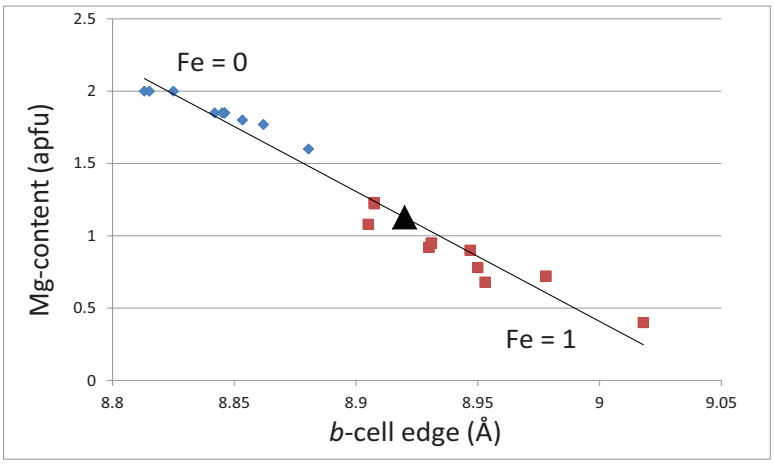

Fig. S4a

Variation of Mg-content with *b* unit-cell parameter in pigeonite. Blue diamonds represent Fe# = 0 and red squares are Fe# = 1. The estimated Mg# of the Rocknest pigeonite is 1.13 and is marked with the black triangle.

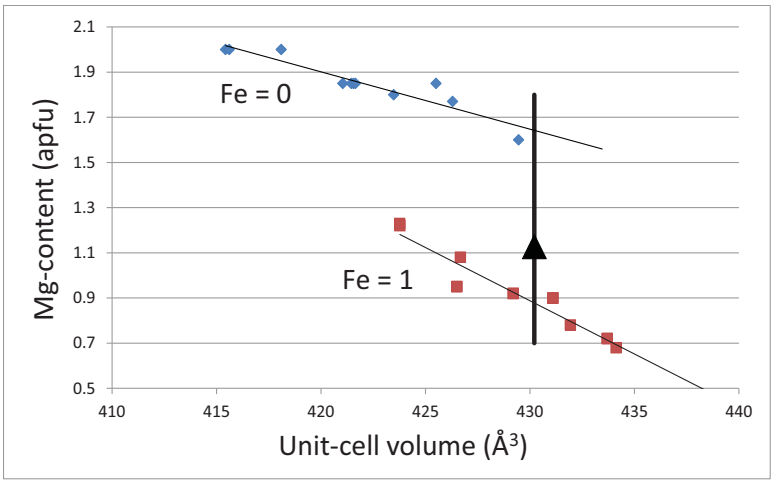

Fig. S4b

Fe-content in pigeonite - from the Mg-content determined above and scaling between the trends of samples with no Fe (blue diamonds) and Fe# = 1 (red squares), the Rocknest pigeonite is estimated to contain 0.68 apfu Fe.

Table S2.

Oxide wt. % compositions of the crystalline mineral phases present in the <150 μm size fraction of Rocknest sediment

	augite	olivine	plagioclase	pigeonite	magnetite	hematite	ilmenite	sanidine	quartz	anhydrite	Total
SiO_2	53.58	36.49	53.81	53.36	0	0	0	64.76	100	0	48.66
TiO_2	0	0	0	0	0	0	52.65	0	0	0	0.37
Al_2O_3	0	0	29.50	0	0	0	0	18.32	0	0	13.04
FeO	11.85	33.16	0	21.69	87	100	47.35	0	0	0	13.95
MnO	0	0	0	0	0	0	0	0	0	0	0.00
MgO	15.81	30.35	0	20.22	0	0	0	0	0	0	11.17
CaO	18.75	0	11.78	4.73	0	0	0	0	0	41.19	9.30
Na_2O	0	0	4.91	0	0	0	0	0	0	0	2.11
K_2O	0	0	0	0	0	0	0	16.92	0	0	0.36
SO_3	0	0	0	0	0	0	0	0	0	58.81	0.82
Component	0.146	0.224	0.408	0.138	0.021	0.011	0.009	0.013	0.014	0.015	

List of the members of the Mars Science Laboratory Science Team

Achilles, Cherie	Jacobs Technology (at NASA JSC)
Agard, Christophe	CNES (Centre National d'Etudes Spatiales)
Alves Verdasca, José Alexandre	CAB (Centro de Astrobiología)
Anderson, Robert	NASA JPL
Anderson, Ryan	USGS Flagstaff
Archer, Doug	NASA Postdoc Program (at NASA JSC)
Armiens-Aparicio, Carlos	CAB (Centro de Astrobiología)
Arvidson, Ray	WUSTL (Washington University in St. Louis)
Atlaskin, Evgeny	FMI (Finnish Meteorological Institute) and University of Helsinki
Atreya, Sushil	University of Michigan Ann Arbor
Aubrey, Andrew	NASA JPL
Baker, Burt	MSSS (Malin Space Science Systems)
Baker, Michael	Caltech
Balic-Zunic, Tonci	University of Copenhagen
Baratoux, David	IRAP (Institut de Recherche en Astrophysique et Planetologie)
Baroukh, Julien	CNES (Centre National d'Etudes Spatiales)
Barraclough, Bruce	PSI (Planetary Science Institute)
Bean, Keri	Texas A&M
Beegle, Luther	NASA JPL
Behar, Alberto	NASA JPL
Bell, James	ASU (Arizona State University)
Bender, Steve	PSI (Planetary Science Institute)
Benna, Mehdi	University of Maryland Baltimore County (at NASA GSFC)
Bentz, Jennifer	University of Saskatchewan
Berger, Gilles	IRAP (Institut de Recherche en Astrophysique et Planetologie)
Berger, Jeff	University of New Mexico (Western Univ. May 1)

Berman, Daniel	PSI (Planetary Science Institute)
Bish, David	Indiana University Bloomington
Blake, David F.	NASA Ames
Blanco Avalos, Juan J.	Universidad de Alcalá de Henares
Blaney, Diana	NASA JPL
Blank, Jen	BAER (at NASA Ames)
Blau, Hannah	University of Massachusetts
Bleacher, Lora	USRA-LPI (at NASA GSFC)
Boehm, Eckart	University of Kiel
Botta, Oliver	Swiss Space Office
Böttcher, Stephan	University of Kiel
Boucher, Thomas	University of Massachusetts
Bower, Hannah	University of Maryland College Park
Boyd, Nick	University of Guelph
Boynton, Bill	University of Arizona
Breves, Elly	Mount Holyoke College
Bridges, John	University of Leicester
Bridges, Nathan	APL (Johns Hopkins University Applied Physics Laboratory)
Brinckerhoff, William	NASA GSFC
Brinza, David	NASA JPL
Bristow, Thomas	NASA Postdoc Program (at NASA Ames)
Brunet, Claude	CSA (Canadian Space Agency)
Brunner, Anna	University of Maryland College Park (at GSFC)
Brunner, Will	inXitu
Buch, Arnaud	LGPM, Ecole Centrale Paris (Laboratoire Génie des Procédés et Matériaux)
Bullock, Mark	SwRI (Southwest Research Institute)
Burmeister, Sönke	University of Kiel
Cabane, Michel	LATMOS (Laboratoire Atmosphères, Milieux, Observations Spatiales)

Calef, Fred	NASA JPL
Cameron, James	Lightstorm Entertainment Inc.
Campbell, John "Iain"	University of Guelph
Cantor, Bruce	MSSS (Malin Space Science Systems)
Caplinger, Michael	MSSS (Malin Space Science Systems)
Caride Rodríguez, Javier	CAB (Centro de Astrobiología)
Carmosino, Marco	University of Massachusetts
Carrasco Blázquez, Isaías	CAB (Centro de Astrobiología)
Charpentier, Antoine	ATOS Origin
Chipera, Steve	Chesapeake Energy
Choi, David	NASA Postdoc Program (at NASA GSFC)
Clark, Benton	SSI (Space Science Institute)
Clegg, Sam	LANL (Los Alamos National Lab)
Cleghorn, Timothy	NASA JSC
Cloutis, Ed	University of Winnipeg
Cody, George	Carnegie Institution of Washington
Coll, Patrice	LISA (Laboratoire Interuniversitaire des Systèmes Atmosphériques), Université Paris
Conrad, Pamela	NASA GSFC
Coscia, David	LATMOS (Laboratoire Atmosphères, Milieux, Observations Spatiales)
Cousin, Agnès	LANL (Los Alamos National Lab)
Cremers, David	ARA (Applied Research Associates, Inc.)
Crisp, Joy	NASA JPL
Cros, Alain	IRAP (Institut de Recherche en Astrophysique et Planetologie)
Cucinotta, Frank	NASA JSC
d'Uston, Claude	IRAP (Institut de Recherche en Astrophysique et Planetologie)
Davis, Scott	MSSS (Malin Space Science Systems)
Day, Mackenzie "Kenzie"	University of Texas at Austin
de la Torre Juarez, Manuel	NASA JPL

DeFlores, Lauren	NASA JPL
DeLapp, Dorothea	LANL (Los Alamos National Lab)
DeMarines, Julia	Denver Museum of Nature & Science
DesMarais, David	NASA Ames
Dietrich, William	University of California Berkeley
Dingler, Robert	LANL (Los Alamos National Lab)
Donny, Christophe	CNES (Centre National d'Etudes Spatiales)
Downs, Bob	University of Arizona
Drake, Darrell	retired
Dromart, Gilles	LGL-TPE (Laboratoire de Géologié de Lyon : Terre, Planète, Environnement)
Dupont, Audrey	CS Systemes d'Information
Duston, Brian	MSSS (Malin Space Science Systems)
Dworkin, Jason	NASA GSFC
Dyar, M. Darby	Mount Holyoke College
Edgar, Lauren	ASU (Arizona State University)
Edgett, Kenneth	MSSS (Malin Space Science Systems)
Edwards, Christopher	Caltech
Edwards, Laurence	NASA Ames
Ehlmann, Bethany	Caltech
Ehresmann, Bent	SwRI (Southwest Research Institute)
Eigenbrode, Jen	NASA GSFC
Elliott, Beverley	University of New Brunswick
Elliott, Harvey	University of Michigan Ann Arbor
Ewing, Ryan	University of Alabama
Fabre, Cécile	G2R (Géologié et Gestion des Ressources Minérales et Energétique)
Fairén, Alberto	Cornell University
Farley, Ken	Caltech
Farmer, Jack	ASU (Arizona State University)

Fassett, Caleb	Mount Holyoke College
Favot, Laurent	Capgemini France
Fay, Donald	MSSS (Malin Space Science Systems)
Fedosov, Fedor	Space Research Institute
Feldman, Jason	NASA JPL
Feldman, Sabrina	NASA JPL
Fisk, Marty	Oregon State University
Fitzgibbon, Mike	University of Arizona
Flesch, Greg	NASA JPL
Floyd, Melissa	NASA GSFC
Flückiger, Lorenzo	Carnegie Mellon University (at NASA Ames)
Forni, Olivier	IRAP (Institut de Recherche en Astrophysique et Planetologie)
Fraeman, Abby	WUSTL (Washington University in St. Louis)
Francis, Raymond	University of Western Ontario
François, Pascaline	LISA (Laboratoire Interuniversitaire des Systèmes Atmosphériques), Université Paris
Franz, Heather	University of Maryland Baltimore County (at NASA GSFC)
Freissinet, Caroline	NASA Postdoc Program (at NASA GSFC)
French, Katherine Louise	MIT
Frydenvang, Jens	University of Copenhagen
Gaboriaud, Alain	CNES (Centre National d'Etudes Spatiales)
Gailhanou, Marc	CNRS (Centre National de la Recherche Scientifique)
Garvin, James	NASA GSFC
Gasnault, Olivier	IRAP (Institut de Recherche en Astrophysique et Planetologie)
Geffroy, Claude	IC2MP (Institut de Chimie des Milieux et Matériaux de Poitiers)
Gellert, Ralf	University of Guelph
Genzer, Maria	FMI (Finnish Meteorological Institute)
Glavin, Daniel	NASA GSFC
Godber, Austin	ASU (Arizona State University)

Goesmann, Fred	Max Planck Institute for Solar System Research
Goetz, Walter	Max Planck Institute for Solar System Research
Golovin, Dmitry	Space Research Institute
Gómez Gómez, Felipe	Centro de Astrobiología
Gómez-Elvira, Javier	Centro de Astrobiología
Gondet, Brigitte	IAS (Institut d'Astrophysique Spatiale)
Gordon, Suzanne	University of New Mexico
Gorevan, Stephen	Honeybee Robotics
Grant, John	Smithsonian Institution
Griffes, Jennifer	Caltech
Grinspoon, David	Denver Museum of Nature & Science
Grotzinger, John	Caltech
Guillemot, Philippe	CNES (Centre National d'Etudes Spatiales)
Guo, Jingnan	SwRI (Southwest Research Institute)
Gupta, Sanjeev	Imperial College
Guzewich, Scott	NASA Postdoc Program (at NASA GSFC)
Haberle, Robert	NASA Ames
Halleaux, Douglas	University of Michigan Ann Arbor
Hallet, Bernard	University of Washington Seattle
Hamilton, Vicky	(SwRI) Southwest Research Institute
Hardgrove, Craig	MSSS (Malin Space Science Systems)
Harker, David	MSSS (Malin Space Science Systems)
Harpold, Daniel	NASA GSFC
Harri, Ari-Matti	FMI (Finnish Meteorological Institute)
Harshman, Karl	University of Arizona
Hassler, Donald	SwRI (Southwest Research Institute)
Haukka, Harri	FMI (Finnish Meteorological Institute)
Hayes, Alex	Cornell University

Herkenhoff, Ken	USGS Flagstaff
Herrera, Paul	MSSS (Malin Space Science Systems)
Hettrich, Sebastian	CAB (Centro de Astrobiología)
Heydari, Ezat	Jackson State University
Hipkin, Victoria	CSA (Canadian Space Agency)
Hoehler, Tori	NASA Ames
Hollingsworth, Jeff	NASA Ames
Hudgins, Judy	Salish Kootenai College
Huntress, Wesley	Retired
Hurowitz, Joel	NASA JPL
Hviid, Stubbe	Max Planck Institute for Solar System Research
Iagnemma, Karl	MIT
Indyk, Steve	Honeybee Robotics
Israël, Guy	CNRS and LATMOS
Jackson, Ryan	LANL (Los Alamos National Lab)
Jacob, Samantha	University of Hawai'i at Manoa
Jakosky, Bruce	University of Colorado Boulder
Jensen, Elsa	MSSS (Malin Space Science Systems)
Jensen, Jaqueline Kløvgaard	University of Copenhagen
Johnson, Jeffrey	APL (Johns Hopkins University Applied Physics Laboratory)
Johnson, Micah	Microtel (at NASA GSFC)
Johnstone, Steve	LANL (Los Alamos National Lab)
Jones, Andrea	USRA-LPI (at NASA GSFC)
Jones, John	NASA JSC
Joseph, Jonathan	Cornell University
Jun, Insoo	NASA JPL
Kah, Linda	University of Tennessee Knoxville
Kahanpää, Henrik	FMI (Finnish Meteorological Institute)

Kahre, Melinda	NASA Ames
Karpushkina, Natalya	Space Research Institute
Kasprzak, Wayne	NASA GSFC
Kauhanen, Janne	FMI (Finnish Meteorological Institute)
Keely, Leslie	NASA Ames
Kemppinen, Osku	FMI (Finnish Meteorological Institute)
Keymeulen, Didier	NASA JPL
Kim, Myung-Hee	USRA (at NASA JSC)
Kinch, Kjartan	University of Copenhagen
King, Penny	ANU (Australian National University)
Kirkland, Laurel	LPI (Lunar and Planetary Institute)
Kocurek, Gary	University of Texas at Austin
Koefoed, Asmus	University of Copenhagen
Köhler, Jan	University of Kiel
Kortmann, Onno	University of California Berkeley
Kozyrev, Alexander	Space Research Institute
Krezoski, Jill	MSSS (Malin Space Science Systems)
Krysak, Daniel	MSSS (Malin Space Science Systems)
Kuzmin, Ruslan	Space Research Institute and Vernadsky Institute
Lacour, Jean Luc	CEA (Commissariat à l'Énergie Atomique et aux Énergies Alternatives)
Lafaille, Vivian	CNES (Centre National d'Etudes Spatiales)
Langevin, Yves	IAS (Institut d'Astrophysique Spatiale)
Lanza, Nina	LANL (Los Alamos National Lab)
Lasue, Jeremie	IRAP (Institut de Recherche en Astrophysique et Planetologie)
Le Mouélic, Stéphane	LPGN (Laboratoire de Planétologie et Géodynamique de Nantes)
Lee, Ella Mae	USGS Flagstaff
Lee, Qiu-Mei	IRAP (Institut de Recherche en Astrophysique et Planetologie)
Lees, David	Carnegie Mellon University (at NASA Ames)

Lefavor, Matthew	Microtel (at NASA GSFC)
Lemmon, Mark	Texas A&M
Lepinette Malvitte, Alain	CAB (Centro de Astrobiología)
Leshin, Laurie	RPI (Rensselaer Polytechnic Institute)
Léveillé, Richard	CSA (Canadian Space Agency)
Lewin-Carpintier, Éric	ISTerre (Institut des Sciences de la Terre)
Lewis, Kevin	Princeton University
Li, Shuai	Brown University
Lipkaman, Leslie	MSSS (Malin Space Science Systems)
Little, Cynthia	LANL (Los Alamos National Lab)
Litvak, Maxim	Space Research Institute
Lorigny, Eric	CNES (Centre National d'Etudes Spatiales)
Lugmair, Guenter	UCSD (University of California San Diego)
Lundberg, Angela	Delaware State University
Lyness, Eric	Microtel (at NASA GSFC)
Madsen, Morten	University of Copenhagen
Mahaffy, Paul	NASA GSFC
Maki, Justin	NASA JPL
Malakhov, Alexey	Space Research Institute
Malespin, Charles	USRA (at NASA GSFC)
Malin, Michael	MSSS (Malin Space Science Systems)
Mangold, Nicolas	LPGN (Laboratoire de Planétologie et Géodynamique de Nantes)
Manhes, Gérard	Retired
Manning, Heidi	Concordia College
Marchand, Geneviève	CSA (Canadian Space Agency)
Marín Jiménez, Mercedes	CAB (Centro de Astrobiología)
Martín García, César	University of Kiel
Martin, Dave	NASA GSFC

Martin, Mildred	Catholic University of America (at NASA GSFC)
Martínez-Frías, Jesús	Centro de Astrobiología
Martín-Soler, Javier	CAB (Centro de Astrobiología)
Martín-Torres, F. Javier	Centro de Astrobiología
Mauchien, Patrick	CEA (Commissariat à l'Énergie Atomique et aux Énergies Alternatives)
Maurice, Sylvestre	IRAP (Institut de Recherche en Astrophysique et Planetologie)
McAdam, Amy	NASA GSFC
McCartney, Elaina	MSSS (Malin Space Science Systems)
McConnochie, Timothy	University of Maryland (at NASA GSFC)
McCullough, Emily	University of Western Ontario
McEwan, Ian	Ashima Research
McKay, Christopher	NASA Ames
McLennan, Scott	SUNY Stony Brook
McNair, Sean	MSSS (Malin Space Science Systems)
Melikechi, Noureddine	Delaware State University
Meslin, Pierre-Yves	IRAP (Institut de Recherche en Astrophysique et Planetologie)
Meyer, Michael	NASA Headquarters
Mezzacappa, Alissa	Delaware State University
Miller, Hayden	Caltech
Miller, Kristen	MIT
Milliken, Ralph	Brown University
Ming, Douglas	NASA JSC
Minitti, Michelle	ASU (Arizona State University)
Mischna, Michael	NASA JPL
Mitrofanov, Igor	Space Research Institute
Moersch, Jeff	University of Tennessee Knoxville
Mokrousov, Maxim	Space Research Institute
Molina Jurado, Antonio	CAB (Centro de Astrobiología)

Moores, John	York University
Mora-Sotomayor, Luis	CAB (Centro de Astrobiología)
Morookian, John Michael	NASA JPL
Morris, Richard	NASA JSC
Morrison, Shaunna	University of Arizona
Mueller-Mellin, Reinhold	University of Kiel
Muller, Jan-Peter	UCL (University College London)
Muñoz Caro, Guillermo	CAB (Centro de Astrobiología)
Nachon, Marion	LPGN (Laboratoire de Planétologie et Géodynamique de Nantes)
Navarro López, Sara	CAB (Centro de Astrobiología)
Navarro-González, Rafael	UNAM (University Nacional Autónoma de México)
Nealson, Kenneth	USC (University of Southern California)
Nefian, Ara	Carnegie Mellon University (at NASA Ames)
Nelson, Tony	LANL (Los Alamos National Lab)
Newcombe, Megan	Caltech
Newman, Claire	Ashima Research
Newsom, Horton	University of New Mexico
Nikiforov, Sergey	Space Research Institute
Niles, Paul	NASA JSC
Nixon, Brian	MSSS (Malin Space Science Systems)
Noe Dobrea, Eldar	PSI (Planetary Science Institute)
Nolan, Thomas	Nolan Engineering (at NASA GSFC)
Oehler, Dorothy	Jacobs Technology (at NASA JSC)
Ollila, Ann	University of New Mexico
Olson, Timothy	Salish Kootenai College
Owen, Tobias	University of Hawai'i at Manoa
Pablo Hernández, Miguel Ángel de	Universidad de Alcalá de Henares
Paillet, Alexis	CNES (Centre National d'Etudes Spatiales)

Pallier, Etienne	IRAP (Institut de Recherche en Astrophysique et Planetologie)
Palucis, Marisa	University of California Berkeley
Parker, Timothy	NASA JPL
Parot, Yann	IRAP (Institut de Recherche en Astrophysique et Planetologie)
Patel, Kiran	Global Science & Technology, Inc. (at NASA GSFC)
Paton, Mark	FMI (Finnish Meteorological Institute)
Paulsen, Gale	Honeybee Robotics
Pavlov, Alex	NASA GSFC
Pavri, Betina	NASA JPL
Peinado-González, Verónica	CAB (Centro de Astrobiología)
Pepin, Robert	University of Minnesota
Peret, Laurent	ATOS Origin
Perez, Rene	CNES (Centre National d'Etudes Spatiales)
Perrett, Glynis	University of Guelph
Peterson, Joe	SwRI (Southwest Research Institute)
Pilorget, Cedric	Caltech
Pinet, Patrick	IRAP (Institut de Recherche en Astrophysique et Planetologie)
Pla-García, Jorge	CAB (Centro de Astrobiología)
Plante, Ianik	USRA (at NASA JSC)
Poitrasson, Franck	CNRS (Centre National de la Recherche Scientifique) and GET (Géosciences Environnement Toulouse)
Polkko, Jouni	FMI (Finnish Meteorological Institute)
Popa, Radu	USC (University of Southern California)
Posiolova, Liliya	MSSS (Malin Space Science Systems)
Posner, Arik	NASA Headquarters
Pradler, Irina	University of Guelph
Prats, Benito	eINFORMe Inc. (at NASA GSFC)
Prokhorov, Vasily	Space Research Institute

Purdy, Sharon Wilson	Smithsonian Institution
Raaen, Eric	NASA GSFC
Radziemski, Leon	Piezo Energy Technologies, Tucson
Rafkin, Scot	SwRI (Southwest Research Institute)
Ramos, Miguel	Universidad de Alcalá de Henares
Rampe, Elizabeth	NASA Postdoc Program (at NASA JSC)
Raulin, François	LISA (Laboratoire Interuniversitaire des Systèmes Atmosphériques), Université Paris
Ravine, Michael	MSSS (Malin Space Science Systems)
Reitz, Günther	DLR (Deutsches Zentrum für Luft- und Raumfahrt)
Rennó, Nilton	University of Michigan Ann Arbor
Rice, Melissa	NASA Postdoc Program (at Caltech)
Richardson, Mark	Ashima Research
Robert, François	(LMCM) Laboratoire de Minéralogie et Cosmochimie du Muséum
Robertson, Kevin	Brown University
Rodriguez Manfredi, José Antonio	CAB (Centro de Astrobiología)
Romeral-Planelló, Julio J.	CAB (Centro de Astrobiología)
Rowland, Scott	University of Hawai'i at Manoa
Rubin, David	USGS Santa Cruz
Saccoccio, Muriel	CNES (Centre National d'Etudes Spatiales)
Salamon, Andrew	MSSS (Malin Space Science Systems)
Sandoval, Jennifer	MSSS (Malin Space Science Systems)
Sanin, Anton	Space Research Institute
Sans Fuentes, Sara Alejandra	CAB (Centro de Astrobiología)
Saper, Lee	MSSS (Malin Space Science Systems)
Sarrazin, Philippe	inXitu
Sautter, Violaine	LMCM (Laboratoire de Minéralogie et Cosmochimie du Muséum)
Savijärvi, Hannu	University of Helsinki
Schieber, Juergen	Indiana University Bloomington

Schmidt, Mariek	Brock University
Schmidt, Walter	FMI (Finnish Meteorological Institute)
Scholes, Daniel "Dan"	WUSTL (Washington University in St. Louis)
Schoppers, Marcel	NASA JPL
Schröder, Susanne	IRAP (Institut de Recherche en Astrophysique et Planetologie)
Schwenzer, Susanne	Open University
Sebastian Martinez, Eduardo	CAB (Centro de Astrobiología)
Sengstacken, Aaron	NASA JPL
Shterts, Ruslan	Space Research Institute
Siebach, Kirsten	Caltech
Siili, Tero	FMI (Finnish Meteorological Institute)
Simmonds, Jeff	NASA JPL
Sirven, Jean-Baptiste	CEA (Commissariat à l'Énergie Atomique et aux Énergies Alternatives)
Slavney, Susie	WUSTL (Washington University in St. Louis)
Sletten, Ronald	University of Washington Seattle
Smith, Michael	NASA GSFC
Sobrón Sánchez, Pablo	CSA (Canadian Space Agency)
Spanovich, Nicole	NASA JPL
Spray, John	University of New Brunswick
Squyres, Steven	Cornell University
Stack, Katie	Caltech
Stalport, Fabien	LISA (Laboratoire Interuniversitaire des Systèmes Atmosphériques)
Steele, Andrew	Geophysical Lab, Carnegie Institution of Washington
Stein, Thomas	WUSTL (Washington University in St. Louis)
Stern, Jennifer	NASA GSFC
Stewart, Noel	Salish Kootenai College
Stipp, Susan Louise Svane	University of Copenhagen
Stoiber, Kevin	MSSS (Malin Space Science Systems)

Stolper, Ed	Caltech
Sucharski, Bob	USGS Flagstaff
Sullivan, Rob	Cornell University
Summons, Roger	MIT
Sumner, Dawn	University of California Davis
Sun, Vivian	Brown University
Supulver, Kimberley	MSSS (Malin Space Science Systems)
Sutter, Brad	Jacobs Technology (at NASA JSC)
Szopa, Cyril	LATMOS (Laboratoire Atmosphères, Milieux, Observations Spatiales)
Tan, Florence	NASA GSFC
Tate, Christopher	University of Tennessee Knoxville
Teinturier, Samuel	LATMOS (Laboratoire Atmosphères, Milieux, Observations Spatiales)
ten Kate, Inge	Utrecht University
Thomas, Peter	Cornell University
Thompson, Lucy	University of New Brunswick
Tokar, Robert	Planetary Science Institute
Toplis, Mike	IRAP (Institut de Recherche en Astrophysique et Planetologie)
Torres Redondo, Josefina	CAB (Centro de Astrobiología)
Trainer, Melissa	NASA GSFC
Treiman, Allan	(LPI) Lunar and Planetary Institute
Tretyakov, Vladislav	Space Research Institute
Urqui-O'Callaghan, Roser	CAB (Centro de Astrobiología)
Van Beek, Jason	MSSS (Malin Space Science Systems)
Van Beek, Tessa	MSSS (Malin Space Science Systems)
VanBommel, Scott	University of Guelph
Vaniman, David	PSI (Planetary Science Institute)
Varenikov, Alexey	Space Research Institute
Vasavada, Ashwin	NASA JPL

Vasconcelos, Paulo	University of Queensland
Vicenzi, Edward	Smithsonian Institution
Vostrukhin, Andrey	Space Research Institute
Voytek, Mary	NASA Headquarters
Wadhwa, Meenakshi	ASU (Arizona State University)
Ward, Jennifer	WUSTL (Washington University in St. Louis)
Webster, Chris	NASA JPL
Weigle, Eddie	Big Head Endian LLC
Wellington, Danika	ASU (Arizona State University)
Westall, Frances	CNRS (Centre National de la Recherche Scientifique)
Wiens, Roger Craig	LANL (Los Alamos National Lab)
Wilhelm, Mary Beth	NASA Ames and Georgia Institute of Technology
Williams, Amy	University of California Davis
Williams, Joshua	University of New Mexico
Williams, Rebecca	PSI (Planetary Science Institute)
Williams, Richard B. "Mouser"	LANL (Los Alamos National Lab)
Wilson, Mike	UCSF (University of California San Francisco) (at NASA Ames)
Wimmer-Schweingruber, Robert	University of Kiel
Wolff, Mike	SSI (Space Science Institute)
Wong, Mike	University of Michigan Ann Arbor
Wray, James	MSSS (Malin Space Science Systems)
Wu, Megan	MSSS (Malin Space Science Systems)
Yana, Charles	CNES (Centre National d'Etudes Spatiales)
Yen, Albert	NASA JPL
Yingst, Aileen	PSI (Planetary Science Institute) (at University of Wisconsin)
Zeitlin, Cary	SwRI (Southwest Research Institute)
Zimdar, Robert	MSSS (Malin Space Science Systems)
Zorzano Mier, María-Paz	CAB (Centro de Astrobiología)